American Mineralogist, Volume 71, pages 1170–1177, 1986

Studies of unoccupied molecular orbitals of the B–O bond by molecular orbital calculations, X-ray absorption near edge, electron transmission, and NMR spectroscopy

J. A. TOSSELL
Department of Chemistry, University of Maryland, College Park, Maryland 20742, U.S.A.

ABSTRACT

The nature of the unoccupied molecular orbitals (MOs) associated with the B–O bond in gas-phase molecules and solids is determined by performing molecular orbital calculations using the Multiple Scattering Xα molecular orbital method and by comparison of the calculated properties with those obtained from X-ray absorption near-edge spectroscopy (XANES) and electron-transmission spectroscopy (ETS). For three-coordinate B, the lowest-energy unoccupied MO is essentially a B2$p\pi$ nonbonding or weakly antibonding orbital of a_2 symmetry (within the D_{3h} point group). In $B(OH)_3$, this orbital is less stable than its analogue in the isoelectronic gas-phase molecule BF_3 by about 3 eV, and its energy changes only slowly with B–O distance. It generates an absorption about 4 eV below the B1s IP in XANES and a scattering resonance about 4 eV above threshold in ETS. It is the final state for the lowest-energy UV absorptions of the BO_3^{3-} group, and excitations to it from the e' B–O bonding MO dominate the paramagnetic contribution to the ^{11}B nuclear magnetic resonance (NMR) chemical shift. The only other unoccupied orbital observed for three-coordinate B is the e' B–O antibonding orbital that appears above threshold in both XANES and ETS. The energy of this e' antibonding orbital is highly distance dependent and thus may provide useful information on B–O distance in amorphous materials. For four-coordinate B, the lowest-energy unoccupied orbitals lie just above threshold in XANES, giving a qualitatively different spectrum than that of the three-coordinate borates. Parallels are drawn between the properties of the solid borates and those of isoelectronic gas-phase analogues like BF_3 and CF_4. The experimental ETS is reported for $B(OCH_3)_3$, a gas-phase analogue of the BO_3^{3-} group.

INTRODUCTION

B can display either three- or four-coordination with O in borate minerals, and the linkages of the borate polyhedra are often complex (Christ and Clark, 1977). Even greater structural complexity is found in borate glasses, and many spectral techniques have been employed to determine their structural properties (Pye et al., 1978). Mozzi and Warren (1970) established the presence of boroxol groups (B_3O_3 rings) in vitreous B_2O_3 by X-ray diffraction, and Jellison and Bray (1976) used B and O NMR to establish the presence of such boroxol groups in B_2O_3 and to establish the existence of a multiplicity of tetrahedral and trigonal B sites in the alkali borates. The diagnostic parameter in the B NMR spectrum is not the isotropic chemical shift, which is almost the same for three- and four-coordinate B, but the nuclear quadrupole coupling constant, which is very large for three-coordinate B and near zero for the four-coordinate case. Snyder et al. (1976) and Snyder (1978) have calculated quadrupole coupling constants from ab initio self-consistent-field (SCF) MO calculations using moderately large expansion basis sets. Their results were in reasonable quantitative agreement with experiment for $B(OH)_3$ and BF. Gupta and Tossell (1981, 1983) have used ab initio MO calculations to obtain equilibrium B–O bond distances and B–O–B bond angles for a number of monomeric and oligomeric three- and four-coordinate B–O species and to interpret the photoelectron and X-ray emission spectra of B_2O_3.

X-ray absorption spectroscopy has recently been used to determine structural properties of both crystalline and vitreous materials. The oscillations in X-ray absorption in cross section that occur far above the absorption edge or core electron IP are known as the extended X-ray absorption fine structure (EXAFS), and their spacing is determined by the interatomic separations (Teo, 1980). Absorption features just below and just above the core electron IP are known as X-ray absorption near-edge structure (XANES, Sandstrom and Lytle, 1979), and they also contain information on both geometric and electronic structure local to the absorbing atom. Typical applications of XANES to solids utilize a "fingerprinting" approach in which XANES are obtained for well-characterized crystalline solids that are then used as models for the assignment of the measured XANES of poorly characterized materials such as

0003–004X/86/0910–1170$02.00

glasses (Sandstrom et al., 1980; McKeown et al., 1986). It has also been shown for gas-phase molecules that a simple relationship often exists between the energies of XANES peaks arising from sigma antibonding MOs and the corresponding bond distances (Sette et al., 1984, and references therein).

XANES have recently been obtained for some solids containing B–O bonds by Hallmeier et al. (1981). For compounds containing three-coordinate B, they observed a strong absorption lying well below the B1*s* IP and a second strong broader absorption lying above the IP (in the continuum). For the four-coordinate compounds only a single peak just above the B1*s* IP was observed. Hallmeier et al. (1981) interpreted their results on the basis of Multiple Scattering (MS) Xα calculations (Johnson, 1973) on the ground states of BF_3, BF_4^- and CF_4. The state lying below threshold for three-coordinate B was identified as the B2*p* non-bonding state of a_2'' symmetry (within the D_{3h} point group), and the states just above threshold for four-coordinate B were identified as the a_1 and t_2 B–O sigma antibonding states. The observed stabilization of these states in going from BF_4^- to CF_4 was properly reproduced by their calculations. However, they did not explicitly assign the feature in the continuum for three-coordinate B, and they did not obtain absolute XANES energies by the preferred-transition-state approach (Slater, 1972) or calculate intensities in either the bound-state or continuum parts of the spectrum.

Such calculations have been performed for the isoelectronic gas-phase molecule BF_3 by Swanson et al. (1981) and by Tossell et al. (1986) using the bound-state and continuum (Dill and Dehmer, 1974; Davenport et al., 1978) versions of the MS-Xα method and by Schwarz et al. (1983) and Ishiguro et al. (1982) using Hartree-Fock–based methods. All of the above calculations assign the narrow intense feature about 7 eV below the B1*s* IP to an orbital of a_2'' symmetry of B2$p\pi$ character and the broader intense peak about 2 eV above the B1*s* IP to an orbital of *e'* symmetry, which is B–F sigma antibonding. Features attributable to these orbitals have also been observed in the electron-impact vibrational excitation spectrum of BF_3 (Tronc et al., 1982) and in its electron-transmission spectrum (Tossell et al., 1986). In such spectra, which both involve the formation of temporary negative ions, both the a_2'' and *e'* peaks occur above threshold (zero energy for the incident electron). These temporary negative-ion states thus lie above the energy of the neutral molecule plus a free electron.

Solids containing B in three coordination with O may be modeled by a number of different discrete molecules and molecular clusters. We can expect that three-coordinate borates will have many spectral features that are qualitatively the same as those of BF_3, but there may well be important quantitative differences due to the different bonding characters of O and F. Relevant solid borates and a number of different models for them are shown in Figure 1. $B(OCH_3)_3$ is a stable gas-phase molecule that has B–O bonds, but it possesses low symmetry and its spectral properties may be complicated by the presence of the $-CH_3$ groups. Later in this paper we will present the electron-transmission spectrum of $B(OCH_3)_3$ (Fig. 5) and will show that it can be approximated as a combination of the spectral features of $B(OH)_3$ and CH_4. The BO_3^{3-} molecular anion has been used by Gupta and Tossell (1981) to model the photoelectron and X-ray emission spectra of B_2O_3 with reasonably good results. Similar calculations on gas-phase B halides also gave good agreement with photoelectron spectra (Preston et al., 1976). The BO_3^{3-} calculations employed a stabilizing sphere of charge to compensate for the negative charge on the cluster. This procedure stabilizes all the molecular orbitals by about the same amount so that energies for transitions between one orbital and another are well described. However, it is difficult to get accurate absolute ionization potentials using this approach—only relative IPs can be accurately calculated. To calculate accurate XANES energies with respect to the core IP, we need accurate absolute values of the core IP. This problem can be eliminated if we use a neutral cluster. The simplest possible cluster is $B(OH)_3$, which gives both accurate absolute core IPs and reasonable B–O bond distances (Gupta and Tossell, 1983). The equilibrium structure calculated for gas-phase $B(OH)_3$ is of C_{3h} symmetry, with a B–O–H angle of 121°, similar to that observed in solids. However, it is much simpler to perform the calculations on D_{3h} symmetry $B(OH)_3$, and the results should not be qualitatively changed. We shall therefore use the higher-symmetry structure in this paper.

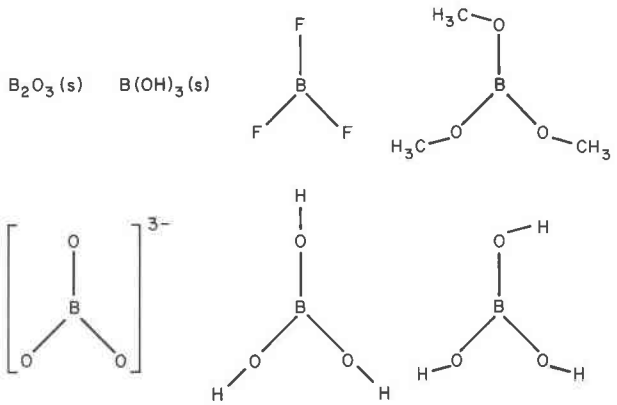

Fig. 1. Compounds and molecular cluster models for 3-coordinate B.

Computational method

The SCF Xα method is a computationally efficient, non-empirical molecular orbital method based on the division of matter into component polyatomic clusters (Johnson, 1973). For example, the simplest SCF Xα model for B_2O_3 is BO_3^{3-}.

The basic steps in the method are as follows:

1. The space within and around the cluster is geometrically partitioned into three contiguous regions, namely, (a) the atomic regions, spherical regions centered on each of the atomic nuclei and overlapping along the metal–ligand axis, (b) the interatomic region, the region outside the atomic regions but within an "outer

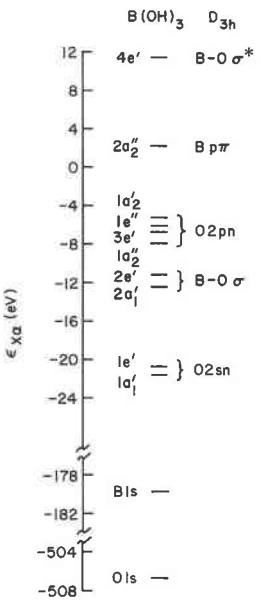

Fig. 2. MS-Xα molecular orbital energy level diagram for the ground state of $B(OH)_3$ in D_{3h} symmetry with a B–O distance of 1.361 Å.

sphere" enclosing all the atomic spheres, and (c) the extramolecular region, the region beyond the "outer sphere."

2. The potential energy at each point is then evaluated, using electrostatics to calculate the Coulomb part of the potential and the Xα statistical approximation of Slater (1972) to evaluate the exchange-correlation contribution. The Xα approximation employs a proportionality between the exchange-correlation potential at a point and the cube root of the density of like-spin electrons at that point. The proportionality constant, α, in this approximation is determined from first principles for the component-free atoms, these α values then being transferred to the corresponding atomic regions of the cluster. Appropriately weighted values of α are used in the interatomic and extramolecular regions.

3. The potential is simplified to a *muffin-tin* form by spherical averaging in the atomic and extramolecular regions and volume averaging in the interatomic region.

4. The one-electron Schrödinger equation is solved numerically in each region, and the solutions are expanded in a rapidly convergent composite partial-wave representation.

5. The wavefunctions and their first derivatives are joined continuously throughout the various regions of the cluster using multiple-scattered-wave theory.

6. The spatial distribution of the electron density is calculated and is used to generate a new potential for the next step in the iterative process. The entire numerical procedure is repeated in successive iterations until self-consistency is attained.

7. The final self-consistent solution for the ground state of the cluster is expressed in terms of one-electron molecular orbitals. These are characterized by their orbital energies (or eigenvalues), by their occupation numbers, and by their electron density distributions.

The SCF Xα method differs from the more familiar Hartree-Fock LCAO-MO method (linear combination of atomic orbitals) in two very important ways. First, in the SCF Xα approach, the Schrödinger equation is solved numerically rather than by expansion in a finite analytical atomic orbital basis set. LCAO methods require the choice of a finite basis set of atomic orbitals and the size of the basis set seriously affects the accuracy of the results. Second, in Hartree-Fock theory, as a result of the HF treatment of the exchange potential, the empty orbitals are treated as "virtual" orbitals that encounter their own self-repulsion and are therefore somewhat too diffuse. In the SCF Xα method, the filled and empty orbitals are treated equivalently by the Xα approximation so that the empty orbitals are good representations of excited-state orbitals.

To obtain excitation energies within the MS-Xα method, self-consistency is obtained for a "transition-state" with orbital occupation numbers intermediate between the initial and final states (Slater, 1972). Procedures for evaluation of spectral intensities for bound-state transitions have been described by Noodleman (1976). For continuum states, solution of the MS-Xα equations is more difficult since one can no longer assume that the wavefunctions decay to zero in the extramolecular region. Also, there is not complete agreement on which set of orbital occupation numbers, e.g., ground state vs. core ionization transition state, should be used to construct the potential for the continuum calculation. The formalism of the continuum MS-Xα method has been described in detail by Dill and Dehmer (1974).

Results

Orbital energies of $B(OH)_3$

The molecular orbital energy level diagram for $B(OH)_3$ for ground state of D_{3h} symmetry with a B–O distance of 1.361 Å and an O–H distance of 0.96 Å is shown in Figure 2. Standard choices were made for alpha parameters (Schwarz, 1972) and atomic sphere radii (Norman, 1974). The highest-energy occupied molecular orbital (HOMO) is the $1a_2''$, which is O2$p\pi$ nonbonding in character. The calculated IP for the orbital is 11.2 eV, which compares well with the HOMO IP of 10.4 eV measured for $B(OCH_3)_3$ (Kroner et al. 1973). The width of the upper valence region in $B(OCH_3)_3$ is also close to that measured for B_2O_3 (Joyner and Hercules, 1980; 7.3 eV in $B(OCH_3)_3$ vs. 7.5 eV in B_2O_3). The lowest-energy unoccupied orbitals localized on the B and O atoms are the $2a_2''$ and $4e'$ orbitals, which are respectively B2$p\pi$ nonbonding and B–O sigma antibonding, although the $2a_2''$ has some O2$p\pi$ with antibonding character mixed in. These are the analogues of the BF_3 unoccupied orbitals. There are also a number of very diffuse or Rydberg-like orbitals not shown in Figure 2. Such diffuse orbitals are not expected to exist in a solid, so they are not important in interpretation of the XANES of borates. In fact, the Rydberg nature of such orbitals is often identified by their disappearance in going from the gas-phase to the solid-state spectrum (Friedrich, et al., 1980).

XANES

Energies and intensities for excitation of states lying below the B1*s* IP can be obtained by using the transition-state method to obtain the energy difference and the method of Noodleman (1976) to obtain the transition intensity. In the transition-state method, self-consistency is obtained for an electron configuration with orbital occupa-

Table 1. Term energies (in eV) of empty $4e'$ (B–$X\sigma^*$) and $2a_2''$ (B$p\pi$) orbitals in BF_3 and $B(OH)_3$

Orbital	BF_3	$B(OH)_3$
$4e'$	−1.8 (−2.3)	−5.1 (−4.1)
$2a_2''$	8.4 (7.2)	4.0 (4.2)

Note: R(B–O) = 1.361 Å, experimental values in parentheses from Hallmeier et al., 1981, bound transition-state calculations used.

tion numbers intermediate between the initial and final states. For example, the B1s–$2a_2''$ excitation energy is obtained as the eigenvalue difference in a state with 1.5 electrons in the B1s and 0.5 electrons in the $2a_2''$ orbital. The corresponding transition state for B1s ionization has 1.5 electrons in the B1s and has the $2a_2''$ empty. Such a bound-state approach can also be used to evaluate excitation energies and intensities to orbitals lying in the continuum, although such a procedure is not formally correct. The correct calculation for this case is the continuum MS-Xα calculation. However, previous experience has shown that when the orbital involved is reasonably well localized in space and lies fairly close to threshold, the two approaches give peak energies that differ by only a few tenths of 1 eV and intensities that are similar (Tossell and Davenport, 1984; Tossell et al., 1986). Direct comparison of intensities in the bound and continuum parts of the spectrum can only be semiquantitative because of difficulty in choosing the half-width of the bound-state transitions (Dehmer and Dill, 1977). We have applied both bound-state and continuum methods to calculation of the XANES of $B(OH)_3$.

In Table 1 we report energies for transitions to the $4e'$ and $2a_2''$ orbitals of BF_3 and $B(OH)_3$ with respect to the B1s IP. Our convention is that orbitals lying below the B1s IP have positive values of "term energy" whereas those lying in the continuum have negative term energies. We include in parentheses the experimental term energies from Ishiguro et al. (1982) and Hallmeier et al. (1981). The absolute term energies calculated are in reasonable agreement with experiment, and the change from BF_3 to $B(OH)_3$ is reproduced accurately. In Figure 3 we show the calculated cross section for the continuum part of the XANES of $B(OH)_3$ obtained from a continuum MS-Xα calculation using the B1s→$2a_2''$ transition-state potential. The maximum occurs at 6.8 eV, about 1.7 eV higher than the $4e'$ orbital energy obtained from the bound-state calculation. Thus, the simpler bound-state method gives results comparable to the formally correct scattering calculation. In Table 2 we report oscillator strengths for the transitions from the B1s core to the $2a_2''$ and $4e'$ orbitals, obtained using the bound-state approach and the intensity formalism of Noodleman (1976). For BF_3 the MS-Xα results are in good agreement with the Hartree-Fock results and in reasonable agreement with experiment. Assuming a full width at half maximum of 2 eV, the calculated oscillator strength of the B1s–$4e'$ transition in BF_3 corresponds to

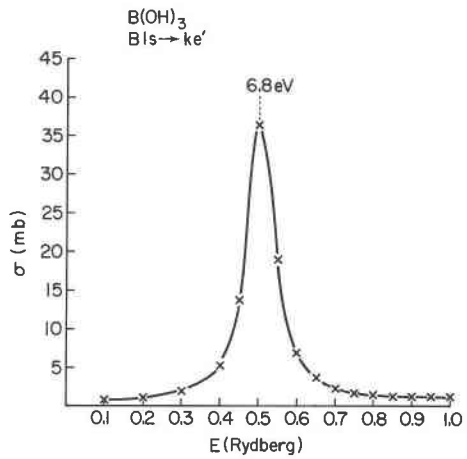

Fig. 3. MS-Xα calculated B1s → ke' photoabsorption cross sections for $B(OH)_3$ with a B–O distance of 1.361 Å.

a cross section of about 4.4 Mb, compared to a cross-section maximum of 5.6 Mb from the continuum calculation. However, the experimental $4e'$ peak is unexpectedly broad, probably as a consequence of the bond-distance effect we discuss below.

It is apparent from Table 2 that BF_3 and $B(OH)_3$ differ in XANES intensities as well as energies. We can understand this qualitatively by examining the charge distribution for the $2a_2''$ orbitals of the two molecules. The B sphere radii used in BF_3 and $B(OH)_3$ differ by about 8%, but the percentage of the electron density within these spheres differs by almost a factor of two, with that for BF_3 being larger (34% vs. 18%). Since the $2a_2''$ orbital is more localized on the B atom in BF_3, it is reasonable that it will give the larger transition intensity. The delocalization of the $2a_2''$ orbital in $B(OH)_3$ through B–O π antibonding is consistent with its reduced acidity and lower ^{11}B electric-field gradient (Snyder, 1978) compared to BF_3. This orbital is often described as an essentially nonbonding orbital, but there is evidence that even for BF_3, it has significant antibonding character. SCF MO calculations on BF_3^-, with one electron in the $2a_2''$ orbital, give an equilibrium distance about 0.18 Å longer than in BF_3, consistent with antibonding character for this orbital (So, 1977).

We have also calculated the $2a_2''$ and $4e'$ orbital energies of $B(OH)_3$ at B–O distances above and below the experimental value, as shown in Table 3. Both the $2a_2''$ and $4e'$ orbitals are destabilized as the B–O distance decreases.

Table 2. Oscillator strengths for transitions to $2a_2''$ and $4e'$ orbitals in BF_3 and $B(OH)_3$

	BF_3		$B(OH)_3$	
	$2a_2''$	$4e'$	$2a_2''$	$4e'$
MS-Xα calc.	0.105	0.081	0.0493	0.0566
HF calc.*	0.105	0.116	—	—
exp.*	0.082	0.195	—	—

* Ishiguro et al. (1982).

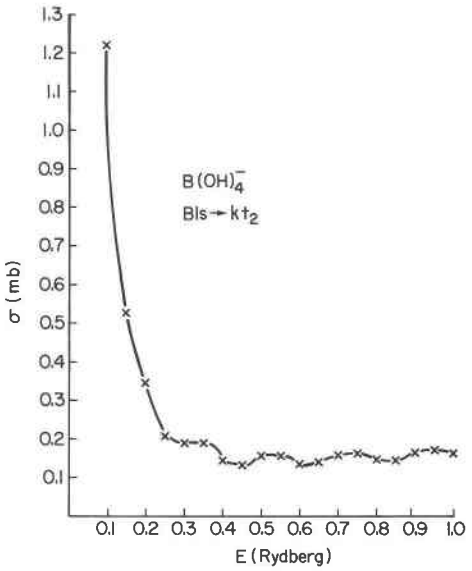

Fig. 4. MS-Xα calculated B1s → kt_2 photoabsorption cross sections for $B(OH)_4^-$ with a B–O distance of 1.472 Å.

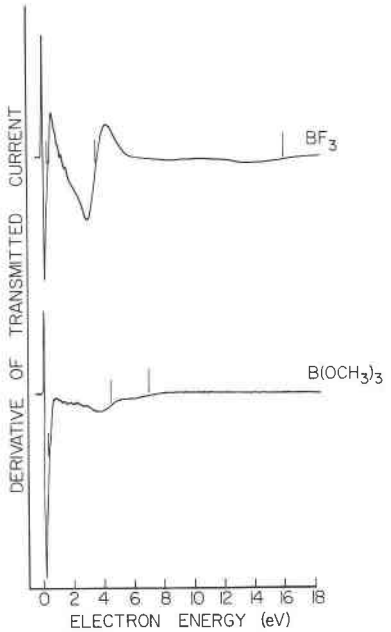

Fig. 5. Derivative-mode electron-transmission spectra of BF_3 and $B(OCH_3)_3$.

The change in the $4e'$ orbital energy is about 24 eV per Å, of the same order of magnitude as that observed by Sette et al. (1984). Such a strong dependence of $4e'$ orbital energy on B–O distance implies that the variation in energy of this feature may be diagnostic of B–O distance. It also indicates that vibrational averaging of the calculated spectrum will be necessary to obtain quantitative agreement with experiment. That is, later continuum calculations of XANES energy and intensity will have to be performed at a range of internuclear distances.

Although we have not carried out a full set of calculations on $B(OH)_4^-$ analogous to those performed on $B(OH)_3$, we have examined some of the possible B1*s*-unoccupied t_2 XANES transitions and have calculated the cross sections for excitation to t_2 symmetry continuum states. MS-Xα calculations were performed on $B(OH)_4^-$ with a B–O distance of 1.47 Å and a Watson sphere potential sufficient to give the same B1*s* IP as for $B(OH)_3$. All transitions from the B1*s* to unoccupied t_2 orbitals giving excitation energies lower than this IP value were considered. In all cases, the t_2 orbitals found were very diffuse, with more than 90% of their electron density in the outer sphere region. Although direct calculations of oscillator strengths were not performed owing to program limitations, our experience indicates that such highly delocalized orbitals always give very small transition intensities. A calculation of continuum cross sections was made as for $B(OH)_3$ using the B1*s* IP transition-state potential, and results are displayed in Figure 4. The cross section shows a maximum as the ionization threshold is approached and a weak oscillatory structure at higher energies. Owing to uncertainties regarding the exact position of the threshold for this anion and neglect of vibrational effects, we can not quantitatively reproduce the XANES typically observed for four-coordinate B. Nonetheless, it is clear that the qualitative form of the spectrum is reproduced by our calculations. That is, the XANES of four-coordinate B has an intense peak just above threshold and no other clear features.

Table 3. Term energies (in eV) of empty $4e'$ (B–Oσ^*) and $2a_2''$ (B$p\pi$) orbitals (with respect to B1*s* ionization threshold) as a function of B–O distance from bound transition-state calculations

	B–O distance		
	1.411 Å	1.361 Å	1.311 Å
$4e'$	−4.0	−5.1	−6.4
$2a_2''$	5.7	5.0	4.3

Table 4. Percentage contributions of orbitals of $B(OH)_3$ to the paramagnetic part of the ^{11}B NMR chemical shielding (using a double zeta basis set)

Oribtal	Type	Percentage of total σ^p_{av}(B)
$1a_2'$	O2$p\pi$	3.8
$1e''$		5.3
$3e'$		2.8
$1a_2''$		9.1
$2e'$	B–Oσ	70.2
$2a_1'$		0.2
$1e'$	O2*sn*	3.1
$1a_1'$		1.1
cores		4.4

Table 5. Calculated energetics of X-ray transitions in $C(OH)_3^+$

Transition	Spectrum	ΔE	C1s IP − ΔE
C1s → $1a_2''$	XES	289.7	16.7
C1s → $2a_2''$	XAS	297.5	8.9
C1s → $4e'$		306.8	−0.4
C1s → continuum		213.6	
destabilization of C1s by $2a_2''$ electron		6.2	
Corrected C1s IP		306.4	

Note: Experimental energy of C1s → $1a_2''$ transition is 279.0 eV (Kosuch et al., 1978).

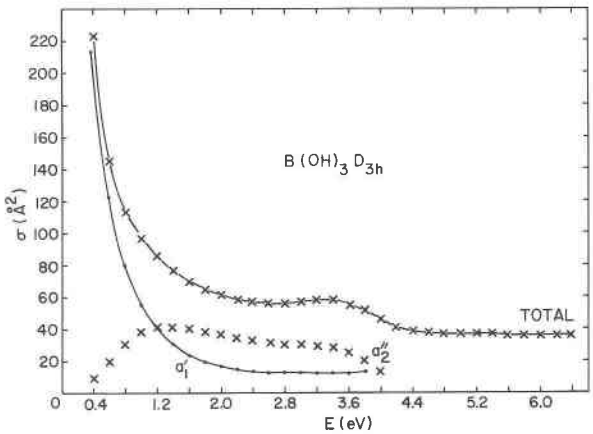

Fig. 6. MS-Xα calculated elastic electron-scattering cross sections for $B(OH)_3$.

ETS

As described above, electron-transmission spectroscopy is a technique complementary to XANES. We have measured the ETS of $B(OCH_3)_3$ using a spectrometer of the type described by Sanche and Schulz (1973). The spectra of $B(OCH_3)_3$ and BF_3 are shown in Figure 5. The experiment is run in an energy-derivative mode so that a resonant increase in electron-scattering cross section appears as a dip followed by a peak. The resonance energy occurs at the point midway between the dip and the peak and is indicated by short vertical lines above the spectral trace in Figure 5. For BF_3 the features at 3.5 eV and at approximately 16 eV correspond to addition of electrons to the $2a_2''$ and $4e'$ orbitals, respectively (Tronc et al. 1982; Tossell et al., 1986). The ETS of $B(OCH_3)_3$ may be interpreted by performing a direct calculation of the elastic electron scattering cross section for $B(OH)_3$ within the continuum MS-Xα approach, which is shown in Figure 6. The ETS feature observed around 4.2 eV probably corresponds to the $2a_2''$ orbital resonance, and the broader feature around 6.8 eV may correspond to the broad resonance around 8 eV observed in CH_4 (Barbarito et al., 1979). The calculated cross section in Figure 6 has an apparent two-peak structure in the a_2'' channel that is connected with the presence of two peripheral scattering centers, O and H. Such an effect is anticipated although its quantitative features are an artifact of the choice of a $B(OH)_3$ model. The replacement of $-CH_3$ by –H in the calculation precludes the CH_4-like feature observed experimentally. Thus, the ETS of $B(OCH_3)_3$ may be seen as a combination of $B(OH)_3$- and CH_4-like features.

UV and NMR spectra

The XANES of borates is important not only as a source of information on the geometries of borate species and the nature of their unoccupied orbitals. It is also of potential value in the interpretation of other spectral properties that involve the unoccupied orbitals. Two such properties are the UV absorption and the ^{11}B NMR chemical shift. Our MS-Xα calculations indicate that the lowest-energy symmetry-allowed transition in $B(OH)_3$ is $1e''$ → $2a_2''$ with an energy of 8.4 eV. The paramagnetic part of the ^{11}B NMR shift is also dominated by transitions into this orbital. The response of a molecule to a magnetic field may be accurately described using the method of coupled Hartree-Fock perturbation theory (CHFPT, Lipscomb, 1966). For a given choice of the origin of the vector potential of the magnetic field, the chemical-shielding tensor can be partitioned into diamagnetic and paramagnetic parts. The diamagnetic part is a quantum mechanical average or expectation value over the ground-state wavefunction alone, and the paramagnetic term involves excitations from the ground state to all possible symmetry-allowed excited states. The paramagnetic term can be divided into contributions from individual occupied orbitals. This procedure has recently been used by Tossell and Lazzeretti (1986) to analyze ^{29}Si NMR shifts. A CHFPT calculation on $B(OH)_3$ (Tossell and Lazzeretti, unpub. results) using a relatively small basis set (double zeta, i.e., two functions for each atomic orbital) shows that the paramagnetic part of the shift is dominated by the $2e'$ B–O sigma bonding orbital from which electrons are excited into the $2a_2''$ orbital. Such a transition is symmetry allowed for the magnetic-field operator, the x and y components of which transform as e'' within the D_{3h} point group. This excitation is of very low energy and therefore makes a very large contribution to the paramagnetic shielding. The complete orbital decomposition of the paramagnetic part of the shielding is given in Table 4.

XANES of related molecules

It is also of interest to extend the XANES analysis to other oxyanions isoelectronic with BO_3^{-3}. MS-Xα calculations on D_{3h} symmetry $C(OH)_3^+$, with a C–O distance of 1.24 Å, give the spectral energies shown in Table 5. Owing to its positive charge, $C(OH)_3^+$ will have a higher C1s IP than would an analogue neutral compound. We can correct for this approximately by subtracting from the calculated C1s IP the destabilization produced by the presence of an additional electron, e.g., one in the $2a_2''$ orbital. Using this correction, we find that both the $2a_2''$ and $4e'$ orbitals have much more positive term energies (i.e., lie farther below the core ionization threshold) than in $B(OH)_3$. Although no XANES is available for CO_3^{2-}, the XANES of

CF_4 (Hallmeier et al., 1981) shows an increase in the term energy of the unoccupied t_2 antibonding orbital of about 4 eV compared to BF_4^-. It thus appears that within an isoelectronic series, an increase in the nuclear charge of the central atom will cause a stabilization of the antibonding orbitals even though the internuclear distance decreases. We therefore anticipate that the XANES of carbonates should show peaks well below the C1*s* ionization threshold from the $2a_2''$ orbital and very near the threshold from the $4e'$ orbital. Other theoretical studies of the XANES of BF_4^- and CF_4 have basically reproduced such a change in term energy although a full explanation of the transition intensities required a consideration of vibrational effects (Schwarz et al., 1983). We note that the XANES of hexagonal BN (Barth et al., 1980) is qualitatively similar to that of $B(OH)_3$ or $C(OH)_3^+$. For this material the B1*s* XANES shows peaks at 192 and 199 eV that may be assigned to orbitals analogous to the $2a_2''$ and $4e'$ orbitals of the discrete gas-phase molecules.

Acidity of boron and carbon oxides

It is well known that three-coordinate B reacts more readily with bases to form four-coordinate compounds than does three-coordinate C. Nonetheless, the $2a_2''$ orbital that accepts electron density from the base actually seems to be more stable for the C than for the B compound. The instability of the four-coordinate species formed by addition of a base to a CO_3 species thus cannot arise from an inherent instability of the acceptor orbital. Rather, repulsions between the entering base and closed electron shells on the other O atoms must cause the destabilization. Consistent with this idea is the large C–O distance observed for four-coordinate compounds such as $C(OCH_3)_4$ (Mijlhoff et al., 1973). The increase in C–O distance from three to four coordination is about 0.16 Å, compared to a typical change of 0.12 Å in B–O distance between three and four coordination (Gupta et al., 1981).

Conclusions

MS-Xα bound-state and continuum calculations substantiate previous qualitative assignments of the XANES of three-coordinate B and yield spectral energies and intensities in semiquantitative agreement with experiment. The B1$s \rightarrow 2a_2''$ spectra intensities indicate a greater B2$p\pi$–O$p\pi$ covalency for the B–O than for the B–F bond. Variations in the energy of the B1$s \rightarrow 4e'$ XANES resonance give information on the B–O bond distance. The effect of change in coordination number and change in central-atom atomic number are correctly reproduced by the calculations. Since excitations to the $2a_2''$ orbital dominate the ^{11}B NMR shift, it may be possible to establish at least a qualitative relationship between NMR shifts and XANES energies.

Acknowledgments

This work was supported by NSF Grants CHE-84-17759 and EAR-82-13115 and by the Computer Science Center, University of Maryland at College Park. I thank J. K. Olthoff and J. H. Moore for obtaining the ETS of $B(OCH_3)_3$.

References

Barbarito, E., Basta, M., and Calicchio, M. (1979) Low energy electron scattering from methane. Journal of Chemical Physics, 71, 54–59.

Barth, J., Kunz, C., and Zimkina, T.M. (1980) Photoemission investigation of hexagonal BN: Band structure and atomic effects. Solid State Communications, 36, 453–456.

Christ, C.L., and Clark, J.R. (1977) A crystal-chemical classification of borate structures with emphasis on hydrated borates. Physics and Chemistry of Minerals, 2, 59–88.

Davenport, J.W., Ho, W., and Schrieffer, J.R. (1978) Theory of vibrationally inelastic electron scattering from oriented molecules. Physical Review, B17, 3115–3127.

Dehmer, J.L., and Dill, D. (1977) Molecular effects on inner-shell photoabsorption. *K*-shell spectrum of N_2. Journal of Chemical Physics, 65, 5327–5334.

Dill, D., and Dehmer, J.L. (1974) Electron-molecule scattering and molecular photoionization using the multiple-scattering method. Journal of Chemical Physics, 61, 693–699.

Friedrich, H., Pittel, B., Rabe, P., Schwarz, W.H.E., and Sonntag, B. (1980) Overlapping core to valence and core to Rydberg transitions and resonances in the XUV spectra of SiF_4. Journal of Physics B: Atomic and Molecular Physics, 13, 25–30.

Gupta, A., and Tossell, J.A. (1981) A theoretical study of bond distances, X-ray spectra and electron density distributions in borate polyhedra. Physics and Chemistry of Minerals, 7, 159–164.

——— (1983) Quantum mechanical studies of distortions and polymerization of borate polyhedra. American Mineralogist, 68, 989–995.

Gupta, A., Swanson, D.K., Tossell, J.A., and Gibbs, G.V. (1981) Calculation of bond distances, one-electron energies and electron density distributions in first-row tetrahedral hydroxy and oxyanions. American Mineralogist, 66, 601–609.

Hallmeier, K.H., Szargan, R., Meisel, A., Hartmann, E., and Gluskin, E.S. (1981) Investigation of core-excited quantum yield spectra of high-symmetry boron compounds. Spectrochimica Acta, 37A, 1049–1053.

Ishiguro, E., Iwata, S., Suzuki, Y., Mikuni, A., and Sasaki, T. (1982) The boron K photoabsorption spectra of BF_3, BCl_3, and BBr_3. Journal of Physics B: Atomic and Molecular Physics, 15, 1841–1854.

Jellison, G.E., Jr., and Bray, P.J. (1976) A determination of the distribution of quadrupole coupling constants in borate glasses using ^{10}B NMR. Solid State Communications, 19, 517–520.

Johnson, K.H. (1973) Scattered-wave theory of the chemical bond. Advances in Quantum Chemistry, 7, 143–185.

Joyner, D.J., and Hercules, D.M. (1980) Chemical bonding and electronic structure of B_2O_3, H_3BO_3 and BN: An ESCA, Auger, SIMS and SXS study. Journal of Chemical Physics, 72, 1095–1108.

Kosuch, N., Tegeler, E., Wiech, G., and Faessler, A. (1978) X-ray spectroscopic studies of the electronic structure of the oxyanions NO_2^-, NO_3^- and CO_3^{2-}. Journal of Electron Spectroscopy and Related Phenomena, 13, 263–272.

Kroner, J., Nolle, D., and Noth, H. (1973) Photoelectrospectroscopic investigations on boron compounds. I. Orbital sequence and charge densities of methylthio and methyloxyboranes. Zeitschrift für Naturforschung, 28b, 416–425 (in German).

Lipscomb, W.N. (1966) The chemical shift and other second-order magnetic and electric properties of small molecules. Advances in Magnetic Resonance, 2, 137–176.

McKeown, D.A., Waychunas, G.A., and Brown, G.E., Jr. (1986) EXAFS study of the coordination environment of Al in a series of silica-rich glasses and selected minerals within the Na_2O-Al_2O_3-SiO_2 system. Journal of Non-crystalline Solids, in press.

Mijlhoff, F.C., Geise, H.J., and Van Schaick, E.J.M. (1973) The molecular structure of tetramethoxymethane in the gas phase:

An electron diffraction study. Journal of Molecular Structure, 20, 393–401.

Mozzi, R.L., and Warren, B.E. (1970) The structure of vitreous boron oxide. Journal of Applied Crystallography, 3, 251–257.

Noodleman, L. (1976) The determination of optical absorption intensities using the Xα scattered wave method. Journal of Chemical Physics, 64, 2343–2349.

Norman, J.G., Jr. (1974) Non-empirical vs. empirical choices for overlapping-sphere radii ratios in SCF-Xα-sw calculations on perchlorate and sulfurdioxide. Molecular Physics, 31, 1191–1198.

Preston, H.J.T., Kaufman, J.J., Keller, J., Danese, J.B., and Connolly, J.W.D. (1976) MS-Xα calculations on boron trihalides and comparison with their photoelectron spectra. Chemical Physics Letters, 37, 55–59.

Pye, L.D., Frechette, V.D., and Kreidl, N.J., Eds. (1978) Borate glasses: Structure, properties and applications. Plenum, New York.

Sanche, L., and Schulz, G.J. (1973) Electron transmission spectroscopy: Resonances in triatomic molecules and hydrocarbons. Journal of Chemical Physics, 58, 479–486.

Sandstrom, D.R., and Lytle, F.W. (1979) Developments in extended X-ray absorption fine structure applied to chemical systems. Annual Review of Physical Chemistry, 30, 215–238.

Sandstrom, D.R., Lytle, F.W., Wei, P.S.P., Greegor, R.B., Wong, J., and Schultz, P. (1980) Coordination of Ti in TiO_2-SiO_2 glass by X-ray absorption spectroscopy. Journal of Non-crystalline Solids, 41, 201–207.

Schwarz, K. (1972) Optimization of the statistical exchange parameter α for the free atom H through Mb. Physics Review, B5, 2466–2468.

Schwarz, W.H.E., Mensching, L., Hallmeier, K.H., and Szargan, R. (1983) *K*-shell excitations of BF_3, CF_4 and MBF_4 compounds. Chemical Physics, 82, 57–65.

Sette, F., Stohr, J., and Hitchcock, A.P. (1984) Correlation between intramolecular bond lengths and *K*-shell σ-shape resonances in gas-phase molecules. Chemical Physics Letters, 110, 517–520.

Slater, J.C. (1972) Statistical exchange correlation in the self-consistent-field. Advances in Quantum Chemistry, 6, 1–92.

Snyder, L.C. (1978) Quantum chemical calculations to model borate glass electronic structure and properties. In L.D. Pye et al., Eds. Borate glasses: Structure, properties and applications. Plenum, New York.

Snyder, L.C., Peterson, G.E., and Kurkjian, C.R. (1976) Molecular orbital calculations of quadrupolar coupling of ^{11}B in molecular modes of glasses. Journal of Chemical Physics, 64, 1569–1573.

So, S.P. (1977) The structure of BF_3^-. Journal of Chemical Physics, 67, 2929.

Swanson, J.R., Dill, D., and Dehmer, J.L. (1981) Shape resonance effects in the photoabsorption spectra of BF_3. Journal of Chemical Physics, 75, 619–624.

Teo, B.K. (1980) Chemical applications of extended X-ray absorption fine structure (EXAFS) spectroscopy. Accounts of Chemical Research, 13, 412–419.

Tossell, J.A., and Davenport, J.W. (1984) MS-Xα calculation of the elastic electron scattering cross sections and X-ray absorption spectra of CX_4 and SiX_4 (X = H,F,Cl). Journal of Chemical Physics, 80, 813–821.

Tossell, J.A., and Lazzeretti, P. (1986) Ab initio calculations of ^{29}Si NMR chemical shifts for some gas-phase and solid-state silicon fluorides and oxides. Journal of Chemical Physics, 84, 369–374.

Tossell, J.A., Moore, J.H., and Olthoff, J.K. (1986) Studies of unoccupied orbitals of BF_3 and BCl_3 by electron transmission spectroscopy and multiple scattering Xα calculations. International Journal of Quantum Chemistry, 29, 1117–1126.

Tronc, M., Malegat, L., Azria, R., and Lecoat, Y. (1982) Shape-resonance-enhanced vibrational excitation of BF_3 by electron impact. Journal of Physics B: Atomic and Molecular Physics, 15, L253–257.

MANUSCRIPT RECEIVED DECEMBER 24, 1985
MANUSCRIPT ACCEPTED MAY 20, 1986